IEEE Access
Multidisciplinary | Rapid Review | Open Access Journal

Received March 4, 2019, accepted March 13, 2019, date of publication March 18, 2019, date of current version April 5, 2019.

Digital Object Identifier 10.1109/ACCESS.2019.2905961

Optimal Tuning of Fractional Order PID Controller for DC Motor Speed Control via Chaotic Atom Search Optimization Algorithm

BARAN HEKIMOĞLU, (Member, IEEE)
Electrical and Electronics Engineering Department, Batman University, 72100 Batman, Turkey
e-mail: baran.hekimoglu@batman.edu.tr

ABSTRACT In this paper, atom search optimization (ASO) algorithm and a novel chaotic version of it [chaotic ASO (ChASO)] are proposed to determine the optimal parameters of the fractional-order proportional+integral+derivative (FOPID) controller for dc motor speed control. The ASO algorithm is simple and easy to implement, which mathematically models and mimics the atomic motion model in nature, and is developed to address a diverse set of optimization problems. The proposed ChASO algorithm, on the other hand, is based on logistic map chaotic sequences, which makes the original algorithm be able to escape from local minima stagnation and improve its convergence rate and resulting precision. First, the proposed ChASO algorithm is applied to six unimodal and multimodal benchmark optimization problems and the results are compared with other algorithms. Second, the proposed ChASO-FOPID, ASO-FOPID, and ASO-PID controllers are compared with GWO-FOPID, GWO-PID, IWO-PID, and SFS-PID controllers using the integral of time multiplied absolute error (ITAE) objective function for a fair comparison. Comparisons were also made for the integral of time multiplied squared error (ITSE) and Zwe-Lee Gaing's (ZLG) objective function as the most commonly used objective functions in the literature. Transient response analysis, frequency response (Bode) analysis, and robustness analysis were all carried out. The simulation results are promising and validate the effectiveness of the proposed approaches. The numerical simulations of the proposed ChASO-FOPID and ASO-FOPID controllers for the dc motor speed control system demonstrated the superior performance of both the chaotic ASO and the original ASO, respectively.

INDEX TERMS DC motor speed control, fractional order PID controller, chaotic atom search optimization algorithm, robustness analysis, transient response.

I. INTRODUCTION

Proportional+integral+derivative (PID) controllers are commonly used in industry to improve both the transient and steady state behaviors of a system [1]. These controllers are known as traditional or integer order controllers [2]. On the other hand, the fractional order PID (FOPID) controller is a generalized version of the traditional PID controller that uses fractional derivative-integral calculus [3]. The FOPID controller has two additional parameters in addition to the traditional PID controller parameters. These parameters are called the proportional gain constant (K_P), the integral gain constant (K_I), the derivative gain constant (K_D), the order of fractional integration (λ) and the order of fractional derivative (μ). This expansion of traditional PID controllers adds robustness and flexibility to the system [4]. The advantages of FOPID controllers compared to traditional PID controllers include: lower steady-state error, less oscillation and overshoot, better response time, robustness to changes in parameters of the controlled system, and insensitivity to disturbing effects [2]–[7]. FOPID controllers are used in applications such as direct current (DC) motor control [2], [8], asynchronous motor drive system [9], DC-DC amplifier converter [10], synchronization and control of chaotic systems [11], and magnetic levitation system [12].

In general, controller parameters tuning is a difficult task and FOPID controllers have five parameters to be set as mentioned before. There are many time domain and frequency domain methods for tuning of FOPID controller parameters [13]. In general, these tuning methods can be classified

The associate editor coordinating the review of this manuscript and approving it for publication was Md Asaduzzaman.

under three headings; rule-based methods, analytical methods and numerical methods [7]. The parameter tuning methods using heuristic optimization algorithms fall into the numerical methods group and have been used by many researchers in the literature. Heuristic optimization methods such as particle swarm optimization (PSO) [14]–[16], dynamic PSO (dPSO) [2], simulated annealing (SA) [17], genetic algorithm (GA) [18] and bacterial swarm optimization (BSO) [19], are some of the example works that are used for FOPID controller parameter tuning. The greatest advantage of heuristic optimization algorithms compared to other methods is their ability to do search in a random and larger field in solution space. In this way, they can converge to optimum or near optimum solutions effectively. However, the convergence properties of heuristic optimization algorithms are strongly connected to the random numbers generated in each algorithm run [20]. Therefore, chaotic sequences are being adopted instead of randomly generated numbers to get better results, which has made the chaotic systems based algorithms as one of the paradigms of modern heuristic optimization [21].

In literature, several algorithms can be found using chaotic sequences to boost the performance of metaheuristic algorithms for solving optimization problems in engineering applications. In [22], three chaotic maps, namely the piecewise linear, logistic, and sinusoidal, are used with kidney-inspired algorithm (KA) for rainfall forecasting, which significantly improved the accuracy and convergence speed of the original KA. In [23], ten chaotic maps, namely the Chebyshev, circle, Gauss/mouse, iterative, logistic, piecewise, sine, singer, sinusoidal and tent, and in [24], four chaotic maps, namely the circle, logistic, piecewise, and tent, are used with salp swarm algorithm (SSA) for feature selection, which maximized the classification accuracy of the original SSA with minimum number of selected features. In [25], ten chaotic maps, namely the Chebyshev, Gauss/mouse, logistic, sine, sinusoidal, circle, iterative, piecewise, singer and tent, are used with grasshopper optimization algorithm (GOA) for global optimization, which significantly boost the performance of the original GOA. In [26], the singer chaotic map is used with whale optimization algorithm (WOA) for parameter estimation of photovoltaic cells, which improved the local minima stagnation avoidance and convergence speed of the original WOA. In [27], ten chaotic maps, namely Chebyshev, circle, Gauss/mouse, iterative, logistic, piecewise, sine, singer, sinusoidal and tent, are used with moth swarm optimization (MSO), which improved the performance of the original MSO in terms of convergence speed. In [28], five chaotic maps, namely the singer, piecewise, logistic, tent and sinusoidal, are used with antlion optimization (ALO) algorithm for feature selection problem. The results showed that the chaotic ALO is efficient in finding an optimal feature subset, which maximized the classification accuracy with minimum number of selected features. In [29], ten chaotic maps, namely Gauss/mouse, Chebyshev, logistic, iterative, piecewise, sine, singer, circle, sinusoidal and tent, are used with biogeography-based optimization (BBO) and improved the performance of the original BBO for both exploration and exploitation. In [30], logistic chaotic map is used with genetic algorithm (GA) for image encryption. In [31], piecewise chaotic map is used with harmony search (HS) algorithm for the flow shop scheduling problem with limited buffers and improved the solution quality and robustness of the original HS algorithm. In [32], logistic chaotic map is applied to the mutualism and commensalism phases of symbiotic organisms search (SOS) algorithm for optimal reactive power dispatch problem in power systems, which gave substantially better results than the other state-of-art algorithms. In [33], ten chaotic maps, namely the Bernoulli, logistic, Chebyshev, circle, cubic, iterative with infinite collapses, piecewise, singer, sinusoidal and tent, are used to regulate a key parameter of grey wolf optimizer (GWO) for constrained benchmark and engineering problems, which clearly outperformed the standard GWO with very good performance in comparison with other algorithms. In [34], ten chaotic maps, namely the logistic, cubic, sine, sinusoidal, singer, circle, iterative, tent, piecewise, and Gauss/mouse, are considered for tuning the main parameter of WOA, which helped in controlling the exploration and exploitation phases of the algorithm and improved the performance of standard WOA significantly. In [35], ten chaotic maps, namely Chebyshev, circle, Gauss/mouse, iterative, logistic, piecewise, sine, singer, sinusoidal, and tent, are embedded into the gravitational constant of gravitational search algorithm (GSA), which improved the performance of the original GSA significantly. In [36], twelve chaotic maps, namely the Chebyshev, circle, Gaussian, intermittency, iterative, Liebovitch, logistic, piecewise, sine, singer, sinusoidal, and tent, are applied to tune the step size of the cuckoos used in the original cuckoo search (CS) algorithm, which significantly enhanced the search ability of the standard CS on most benchmark problems and on sensor selection problem of turbofan engines as an engineering problem. In [37], three chaotic maps, namely circle, singer and tent, are integrated into the krill herd (KH) algorithm, which yielded superior results compared to the original KH in terms of local optima avoidance and convergence speed.

Tuning of controller parameters for DC motor speed control is an observable real world application that is commonly used as a test bed for heuristic optimization algorithms. For the FOPID controller parameter tuning, GWO [38], PSO [39], and constrained PSO (CPSO) [40]; and for the traditional PID controller parameters tuning, GWO [38], [41], [42], invasive weed optimization (IWO) [43], stochastic fractal search (SFS) [44], GA [45], SSA [46], Jaya optimization algorithm (JOA) [47], and ABC [48] are some of the algorithms that have been utilized in literature. In [38], GWO-FOPID and GWO-PID controllers are designed with the objective function of the integral of time multiplied absolute error (ITAE) and compared with IWO-PID [43], PSO-PID [43] and SFS-PID controllers [44]. The results have shown that the GWO-FOPID approach with ITAE objective function yields less settling and rise times with comparable overshoot values in comparison to existing approaches. In [39], PSO-FOPID

controller is designed with four different performance indices, namely, the ITAE, the integral of absolute error (IAE), the integral of squared error (ISE), and the integral of time multiplied squared error (ITSE) and compared with PSO-PID controller. From the results, it is shown that the PSO-FOPID controller has performed better than the PSO-PID controller and the ITAE has given the best results among the other used objective functions. In [40], CPSO-FOPID controller with ITSE objective function has been designed with five different output constraints, which were based on time and frequency response measures such as settling time, overshoot percentage and phase margin. From MATLAB simulation results, it has been shown that CPSO-FOPID controller yields much more efficient performance than Ziegler-Nichols (ZN) based PID controller in terms of settling time, rise time and overshoot percentage. In all of the above mentioned FOPID and PID controllers that are tuned by heuristic optimization algorithms, the proposed approaches have given much better results than those controllers tuned by the classical methods such as ZN, Cohen-Coon (CC), pole placement and phase/gain margin. However, due to the lack of the proposed algorithms they cannot find the optimal parameters of the utilized controller. For instance, GA, PSO and ABC suffer from memory capability and computational burden despite having great potentials to solve many optimization problems. Better results may be achieved with different optimization approaches. However, these algorithms have disadvantages such as local minimum stagnation, early convergence, difficulty in the selection of control parameters and increased calculation time depending on the size of the system studied [49]–[51]. In addition, there is no precise algorithm for the best solution of the controller parameters in a DC motor speed control system. Therefore, studying a new heuristic optimization algorithm is an important and observable problem for researchers.

From the fore-mentioned motivations, in this study, a novel approach based on chaos theory and atom search optimization (ASO) algorithm that is called chaotic ASO (ChASO) is proposed for tuning of controller parameters in a DC motor speed control system. ASO is a recently proposed metaheuristic optimization algorithm that is inspired by basic molecular dynamics, which mathematically models and mimics the atomic motion in nature [52]. Although the original ASO algorithm is simple and easy to implement, it suffers from two main drawbacks, the local minima stagnation and slow convergence speed, which are common to most metaheuristic algorithms. Therefore, in order to overcome these problems, in this paper, a chaotic sequence created by the logistic map will be used instead of the randomly generated numbers in the original ASO algorithm. To the best of author's knowledge, there is no study proposed in literature to improve the ASO with chaotic dynamics. The main contributions of this paper can be summarized as follows:

1) A novel combination of ASO with chaotic logistic map, namely the chaotic ASO (ChASO) is proposed.
2) The proposed ChASO algorithm is applied to six unimodal and multimodal benchmark optimization problems and the results are compared with other algorithms.
3) Not only the proposed ChASO but also the original ASO algorithms are both applied to the parameter tuning problem of FOPID controller for DC motor speed control. This is the first application of ChASO and ASO algorithms in electrical engineering field.
4) The performances of the proposed approaches are compared with other metaheuristic algorithms; namely the grey wolf optimization (GWO) [38], invasive weed optimization (IWO) [43] and stochastic fractal search (SFS) algorithm [44] in terms of the transient response analysis results using the same objective function of ITAE.
5) In addition to the ITAE objective function, two other most commonly used objective functions in literature, the ITSE and ZLG (the time domain based objective function proposed by Zwe–Lee Gaing) [53] are also used to test the effectiveness of the proposed approaches.
6) Comparative transient response analysis, frequency response (Bode) analysis and robustness analysis under DC motor parameter changes are carried out for the proposed ChASO-FOPID approach.

II. THE PROPOSED HEURISTIC OPTIMIZATION ALGORITMS

A. ATOM SEARCH OPTIMIZATION (ASO) ALGORITHM

ASO is a recently proposed physics-inspired, population-based heuristic algorithm that mimics the atomic motion controlled by interaction and constraint forces to design an effective search mechanism for global optimization problems [52]. The total interaction forces acting on the ith atom in dth dimension, which in fact is the vector sum of the repulsion and the attraction exerted from dynamically changing neighbor atoms on ith atom is given as

$$F_i^d(t) = \sum_{j \in Kbest} rand_j F_{ij}^d(t) \tag{1}$$

where $rand_j$ is a random number in the range of [0,1] and $Kbest$ is a subset of atom population, which consist of the first K atoms with the best fitness function values. To make ASO doing more exploration at the early iterations, each atom needs to interact with as many atoms with better fitness values as its K neighbors, and to make algorithm doing more exploitation at final iterations, each atom needs to interact as few atoms with better fitness values as its K neighbors. Therefore, the value of K needs to be gradually decreased with the course of iterations as follows

$$K(t) = N - (N-2) \times \sqrt{\frac{t}{T}} \tag{2}$$

where N is the total number of atoms in an atomic system, t is the current iteration and T is the maximum number

of iterations. F_{ij}^{d} in (1) is the interaction force that the jth best atom exerts on the ith atom in dth dimension. The interaction force is the gradient of Lennard-Jones (L-J) potential, and in order to handle the optimization problems, the revised version of this model with positive attraction and negative repulsion forces [52] is given as

$$F_{ij}^{d} = -\eta(t)\left[2\left(h_{ij}(t)\right)^{-13} - \left(h_{ij}(t)\right)^{-7}\right]\frac{\vec{r}_{ij}}{r_{ij}} \tag{3}$$

where $\eta(t)$ is the depth function for adjusting the repulsion or the attractive regions and $h_{ij}(t) = r_{ij}/\sigma(t)$ is the ratio of the distance between two atoms to the length scale, which is named as the scaled distance between two atoms, in this paper. $\vec{r}_{ij} = \vec{x}_j - \vec{x}_i$ is the position difference vector where $\vec{x}_j = (x_{j1}, x_{j2}, x_{j3})$ is the position vector of the jth atom and $\vec{x}_i = (x_{i1}, x_{i2}, x_{i3})$ is the position vector of the ith atom. Hence, r_{ij} is the Euclidian distance between the ith and the jth atoms and given as

$$\begin{aligned} r_{ij} &= \left\|\vec{x}_j - \vec{x}_i\right\| \\ &= \sqrt{(x_{j1} - x_{i1})^2 + (x_{j2} - x_{i2})^2 + (x_{j3} - x_{i3})^2} \end{aligned} \tag{4}$$

The depth function in (3) is defined as

$$\eta(t) = \alpha\left(1 - \frac{t-1}{T}\right)^{3} e^{-\frac{20t}{T}} \tag{5}$$

where α is the depth weight and equals to 50, in this paper. The interaction force function with different depth values ($\eta = 1, 5, 10, 30,$ and 50) versus the scaled distance (h) ranging from 0.9 to 2 is shown in Fig. 1.

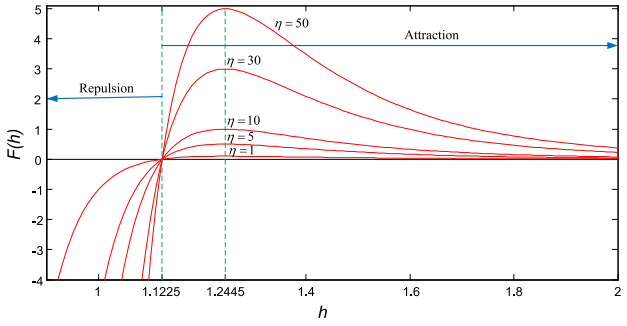

FIGURE 1. The revised interaction force function versus the scaled distance (h) with different depth values (η = 1, 5, 10, 30, and 50) [52].

The scaled distance between two atoms is given as

$$h_{ij}(t) = \begin{cases} h_{\min} & \dfrac{r_{ij}(t)}{\sigma(t)} < h_{\min} \\ \dfrac{r_{ij}(t)}{\sigma(t)} & h_{\min} \le \dfrac{r_{ij}(t)}{\sigma(t)} \le h_{\max} \\ h_{\max} & \dfrac{r_{ij}(t)}{\sigma(t)} > h_{\max} \end{cases} \tag{6}$$

where h_{min} and h_{max} denotes the lover and the upper bounds of the scaled distance (h), respectively, and defined as follows

$$\begin{cases} h_{\min} = g_0 + g(t) \\ h_{\max} = u \end{cases} \tag{7}$$

where g_0 is the lowest limit set to 1.1 and u is the upper limit set to 1.24, and $g(t)$ is the drift factor to make the algorithm capable of drifting from exploration to exploitation, which is given as

$$g(t) = 0.1 \times \sin\left(\frac{\pi}{2} \times \frac{t}{T}\right) \tag{8}$$

The length scale $\sigma(t)$ in (6) denotes the collision diameter and defined as

$$\sigma(t) = \left\| x_{ij}(t), \frac{\sum\limits_{j \in Kbest} x_{ij}(t)}{K(t)} \right\|_2 \tag{9}$$

Supposing that each atom in ASO has a covalent bond with the best atom, the resulting geometric constraint force, which is the weighted position difference between each atom and the best atom, can be given as

$$G_i^d(t) = \lambda(t)\left(x_{best}^d(t) - x_i^d(t)\right) \tag{10}$$

where $x_{best}^d(t)$ is the position of the best atom in dth dimension and $\lambda(t)$ is the Lagrangian multiplier, which is defined as

$$\lambda(t) = \beta e^{-\frac{20t}{T}} \tag{11}$$

where β is a multiplier weight and equals to 0.2, in this paper. Having defined the interaction force and the constraint force resulting from L-J potential and bond-length potential, respectively, the acceleration of the ith atom in dth dimension at iteration t can now be calculated as follows

$$\begin{aligned} a_i^d(t) &= \frac{F_i^d(t)}{m_i^d(t)} + \frac{G_i^d(t)}{m_i^d(t)} \\ &= -\alpha\left(1 - \frac{t-1}{T}\right)^{3} e^{-\frac{20t}{T}} \\ &\quad \times \sum_{j \in Kbest} \frac{rand_j\left[2\left(h_{ij}(t)\right)^{-13} - \left(h_{ij}(t)\right)^{-7}\right]}{m_i(t)} \\ &\quad \cdot \frac{\left(x_j^d(t) - x_i^d(t)\right)}{\left\|\vec{x}_i(t), \vec{x}_j(t)\right\|_2} + \beta e^{-\frac{20t}{T}} \frac{\left(x_{best}^d(t) - x_i^d(t)\right)}{m_i(t)} \end{aligned} \tag{12}$$

where $m_i^d(t)$ is the mass of the ith atom in dth dimension at iteration t, and calculated by its fitness function value as follows

$$M_i(t) = e^{-\frac{Fit_i(t) - Fit_{best}(t)}{Fit_{worst}(t) - Fit_{best}(t)}} \tag{13}$$

$$m_i(t) = \frac{M_i(t)}{\sum_{j=1}^{N} M_j(t)} \tag{14}$$

where $Fit_i(t)$ is the fitness function value of ith atom at iteration t, $Fit_{best}(t)$ and $Fit_{worst}(t)$ are the fitness values of the best and worst atoms at iteration t, respectively, and defined as

$$Fit_{best}(t) = \min_{i \in \{1,2,\ldots,N\}} Fit_i(t) \tag{15}$$

$$Fit_{worst}(t) = \max_{i \in \{1,2,\ldots,N\}} Fit_i(t) \tag{16}$$

TABLE 1. Some benchmark functions.

Name	Definition	Dim (d)	Range	f_{min}
Sphere	$f_1(x)=\sum_{i=1}^{d}x_i^2$	30	[−100, 100]	0
Rosenbrock	$f_2(x)=\sum_{i=1}^{d-1}[100(x_{i+1}-x_i^2)^2+(x_i-1)^2]$	30	[−30, 30]	0
Step	$f_3(x)=\sum_{i=1}^{d}(x_i+0.5)^2$	30	[−100, 100]	0
Rastrigin	$f_4(x)=\sum_{i=1}^{d}[x_i^2-10\cos(2\pi x_i)+10]$	30	[−5.12, 5.12]	0
Ackley	$f_5(x)=-20exp\left(-0.2\sqrt{\frac{1}{d}\sum_{i=1}^{d}x_i^2}\right)-exp\left(\frac{1}{d}\sum_{i=1}^{d}(cos2\pi x_i)\right)+20+e$	30	[−32, 32]	0
Griewank	$f_6(x)=\frac{1}{4000}\sum_{i=1}^{d}x_i^2-\prod_{i=1}^{d}cos\left(\frac{x_i}{\sqrt{i}}\right)+1$	30	[−600, 600]	0

Finally, the velocity and position update of ith atom at iteration $(t+1)$ are defined as

$$v_i^d(t+1) = rand_i^d \cdot v_i^d(t) + a_i^d(t) \quad (17)$$

$$x_i^d(t+1) = x_i^d(t) + v_i^d(t+1) \quad (18)$$

For more detailed explanation of ASO, one can refer to [52].

B. THE NOVEL CHAOTIC ATOM SEARCH OPTIMIZATION (CHASO) ALGORITHM

Chaos has randomness characteristics with better dynamical and statistical characteristics [54]. Small changes in its parameters or initial conditions may lead to vastly different future behaviors [21]. Therefore it is recognized as very useful in metaheuristic optimization algorithms due to the diversity of generated solutions it guarantees. In literature, there are different types of chaotic maps that have been used for generating chaotic sequences in optimization algorithms [20]–[31]. In this paper, a chaotic approach based on the logistic map is proposed. This chaotic map is one of most used [54] and the simplest chaotic sequences that will replace the $rand_j$ parameter of the original ASO algorithm in (1), (12), and (17). The other reason for preferring this map is that it has given the best results after many trials carried out with the piecewise linear map and the sinusoidal map. The logistic map is given by the following expression

$$y_{i+1} = \delta \cdot y_i(1 - y_i) \quad (19)$$

where y is a variable and for $i = 1, 2, 3, \ldots,$ y_i and y_{i+1} are values at ith and $(i+1)$th iterations, respectively. The initial value of y is chosen as 0.2027 [20], in this paper. Here, δ is 4, so that a chaotic sequence of numbers in a range of [0,1] can be generated.

In order to verify the performance of the proposed ChASO algorithm, the six most well-known benchmark functions are discussed. The definitions of these test functions are summarized in Table 1. The detailed information of these functions can also be found in [36] and [52]. In order to make a suitable comparison with other algorithms found in literature, such as wind driven optimization (WDO) [52], SA [52], PSO [52], GSA [52], GA [52] and ASO [52] the proposed ChASO algorithm was run 50 times, and the population size as well as the maximum number of iterations were selected as 50 and 1000, respectively. The statistical results (average, standard deviation and minimum of the best-so-far solution) obtained for the related test functions are presented in Table 2. The best results are highlighted in bold type. As can be seen from the results in Table 2, the best results were found with the proposed ChASO algorithm compared to other algorithms including the original ASO algorithm.

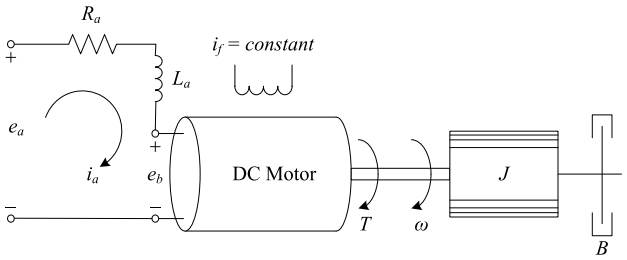

FIGURE 2. DC motor equivalent circuit.

III. DC MOTOR MODEL

DC motors are classified as externally and self-excited types. In this paper, an externally excited DC motor is considered for speed control via the control of armature voltage. The equivalent circuit of DC motor speed control system is shown in Fig. 2 [55].

TABLE 2. Comparison of results for various benchmark functions.

Function	Index	WDO [52]	SA [52]	PSO [52]	GSA [52]	GA [52]	ASO [52]	ChASO (proposed)
$f_1(x)$	Mean	**0**	2.04E−13	0.000146	2.11E−17	0.010212	2.68E−21	1.98E−23
	SD	**0**	6.14E−14	0.000119	6.67E−18	0.005073	3.65E−21	2.42E−22
	Best	**0**	7.76E−14	9.56E−06	1.06E−17	0.002975	3.52E−22	1.83E−24
$f_2(x)$	Mean	28.19528	1059.101	134.3922	28.1473	97.11795	24.8388	**14.96654**
	SD	0.168679	2050.492	128.5852	11.29836	128.7488	**0.515853**	1.898575
	Best	27.95513	23.1826	26.23857	25.75286	9.696092	16.58185	**12.68632**
$f_3(x)$	Mean	0	0.566667	0.133333	0	0	0	**0**
	SD	0	0.727932	0.345746	0	0	0	**0**
	Best	0	0	0	0	0	0	**0**
$f_4(x)$	Mean	57.69854	54.39099	29.31833	15.05704	12.52966	0	**0**
	SD	21.2409	13.82194	6.879953	4.439862	2.915823	0	**0**
	Best	15.56306	26.86388	17.34745	7.959667	6.094298	0	**0**
$f_5(x)$	Mean	8.88E−16	0.343794	0.007432	3.69E−09	0.021188	3.00E−11	**9.85E−17**
	SD	0	0.447427	0.014159	3.96E−10	0.004548	2.15E−11	**7.12E−17**
	Best	8.88E−16	8.29E−08	0.000549	2.96E−09	0.010696	1.13E−11	**4.28E−17**
$f_6(x)$	Mean	0.009891	0.012439	0.022795	4.472721	0.018359	0	**0**
	SD	0.021887	0.010314	0.02737	2.048563	0.009772	0	**0**
	Best	0	3.16E−06	5.88E−05	1.944629	0.006121	0	**0**

The parameters of this system are as follows

R_a: armature resistance, Ω
L_a: armature inductance, H
i_a: armature current, A
i_f: field current, A
e_a: applied armature voltage, V
e_b: back electromotive force, V
T: motor torque, N.m
ω: angular speed of motor shaft, rad/s
J: inertia torque of motor, kg.m2
K_b: electromotive force constant, V.s/rad
K: motor torque constant, N.m/A
B: motor friction constant, N.m.s/rad

For a constant flux, the induced voltage e_b, is proportional to the angular velocity $\omega = d\theta/dt$.

$$e_b = K_b \frac{d\theta}{dt} = K_b \omega \tag{20}$$

The speed of an armature-controlled DC servo motor is controlled by the armature voltage e_a. The differential equation for the armature circuit is as follows

$$e_a = L_a \frac{di_a}{dt} + R_a i_a + e_b \tag{21}$$

The armature current produces a torque that corresponds to the sum of inertia and friction torques, thus

$$T = J \frac{d\omega}{dt} + B\omega = K i_a \tag{22}$$

Note that the load torque is not included in (22) since it is considered as a disturbance to the linear DC motor speed control system. The load disturbance response of the system will be discussed in the last section of simulation results. Assuming that all initial conditions of the system are zero,

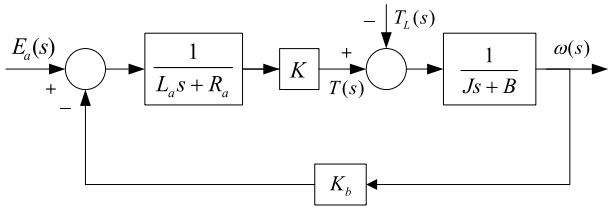

FIGURE 3. DC motor system.

the Laplace transform of (20)-(22) will yield the following equations

$$E_b(s) = K_b \omega(s) \tag{23}$$
$$E_a(s) = (L_a s + R_a) I_a(s) + E_b(s) \tag{24}$$
$$T(s) = (Js + B)\omega(s) = K I_a(s) \tag{25}$$

Fig. 3 illustrates block diagram of a DC motor system. The open loop transfer function of DC motor from input voltage to output motor speed can be written as follows

$$G(s) = \frac{\omega(s)}{E_a(s)} = \frac{K}{(L_a s + R_a)(Js + B) + K_b K} \tag{26}$$

For simulation, the parameters and their values used in the present work for DC motor speed control have been given in Table 3 [38], [43], [44].

TABLE 3. Parameters of DC motor.

Parameter	Value
R_a	0.4 Ω
L_a	2.7 H
J	0.0004 kg.m2
B	0.0022 N.m.s/rad
K	0.015 N.m/A
K_b	0.05 V.s

IV. FOPID CONTROLLER FOR DC MOTOR SPEED CONTROL

A. ESSENTIALS OF FOPID CONTROLLER

A FOPID controller is an extended version of the traditional PID controller. Fractional controllers are less susceptible to changes in the parameters of the supervised system and controller [3], [7]. A fractional controller can very easily obtain iso-damping property that is the system response can have the same phase margin in a given frequency range. The generalized transfer function of FOPID controller is given as follows

$$G_{FOPID}(s) = K_P + K_I s^{-\lambda} + K_D s^{\mu},\ (\lambda, \mu > 0) \quad (27)$$

where K_P, K_I and K_D are proportional, integral and derivative gain constants, respectively, λ is the fractional order of the integral term and μ is the factional order of the derivative term. In general, the range of fractional orders is within 0 to 2 [7]. If $\lambda = 1$ and $\mu = 1$ then the obtained controller is a traditional PID controller; if $\lambda = 0$ and $\mu = 1$, it is a PD controller; if $\lambda = 1$ and $\mu = 0$, it is a PI controller; and if $\lambda = 0$ and $\mu = 0$, it is a P controller. All of these traditional type of controllers are special cases of the FOPID controller. The graphical representation of the FOPID controller is shown in Fig. 4, where x axis represents the fractional order of the integral term while y axis illustrates the fractional order of the derivative term. This figure describes the relationship between the FOPID controller and the standard PID controller. As can be seen from the figure, the FOPID controller extends the integer order PID controller from a point to a plane. This extension adds more flexibility to the controller design, allowing for more accurate control of real-life processes [56].

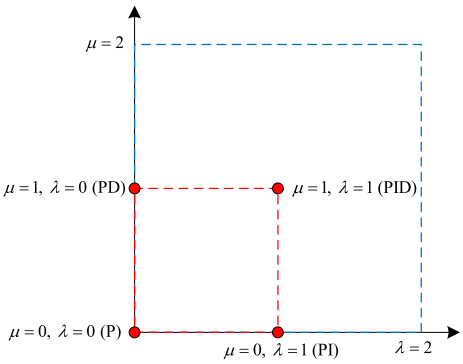

FIGURE 4. The plane of FOPID controller.

B. INTEGER ORDER APPROXIMATION OF FOPID CONTROLLER

In (27), $s^r (r \in -\lambda, \mu)$ is the Laplace transform variable with fractional orders. Since this is an abstract concept, which has no exact analytical solutions, the solution of this variable can only be found with an integer order approximation. Oustaloup's recursive approximation method CRONE [57], is one of the well-known methods of integer order approximation. CRONE is an acronym for 'Commande Robuste d'Ordre Non Entier' in French meaning fractional order robust control. CRONE model [11], [57] with poles and zeros distributed recursively is defined as follows

$$s^r \cong C \prod_{i=1}^{N} \frac{1 + \frac{s}{\omega_{z,i}}}{1 + \frac{s}{\omega_{p,i}}}, \quad r > 0 \quad (28)$$

$$\omega_{z,i} = \omega_l \left(\frac{\omega_h}{\omega_l}\right)^{\frac{(2i-1-r)}{2N}} \quad (29)$$

$$\omega_{p,i} = \omega_l \left(\frac{\omega_h}{\omega_l}\right)^{\frac{(2i-1+r)}{2N}} \quad (30)$$

$$C = \omega_l^r \quad (31)$$

where N is the order of approximation, C is the transient gain, ω_l and ω_h are the low and high transitional frequencies, respectively. In case of $r < 0$, s^r is obtained by inverting (28). However, in case of $|r| > 1$, the above approximation does not yield satisfactory results, which requires the splitting of the fractional order as follows

$$s^r = s^z s^x, \quad r = z + x,\ z \in Z,\ x \in [0, 1] \quad (32)$$

Hence, only the term s^x in (32) has to be approximated.

C. DC MOTOR SPEED CONTROL WITH FOPID CONTROLLER

The block diagram of the closed loop DC motor speed control system using the FOPID controller is shown in Fig. 5. The closed loop transfer function of DC motor with FOPID controller and unity feedback is given as follows

$$T_{FOPID} = \frac{K(K_D s^{\lambda+\mu} + K_P s^{\lambda} + K_I)}{[(Js + B)(Ls + R) + K_b K]s^{\lambda} + K(K_D s^{\lambda+\mu} + K_P s^{\lambda} + K_I)} \quad (33)$$

When designing a controller for DC motor model, two main objectives have been considered. The first one is the preference of a FOPID controller, which is more effective than the traditional PID controller that is mostly used in the literature. And the second one is proposing the ChASO algorithm, which has a better performance than the original ASO algorithm, for tuning FOPID controller parameters (K_P, K_I, K_D, λ and μ). The ChASO-FOPID controller design approach that is based on these two objectives will not only optimize the dynamic response of the DC motor speed control system but also rapidly eliminate its steady-state error.

V. MATHEMATICAL PROBLEM FORMULATION

A. OBJECTIVE FUNCTION AND CONSTRAINTS OF THE PRESENT WORK

In order to present a fair comparison with [38], [43], and [44], the same objective function, ITAE, is adopted in this paper.

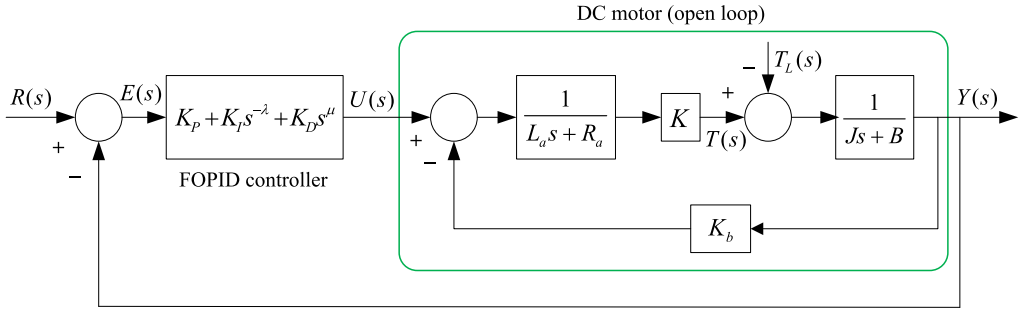

FIGURE 5. Block diagram of DC motor with FOPID controller.

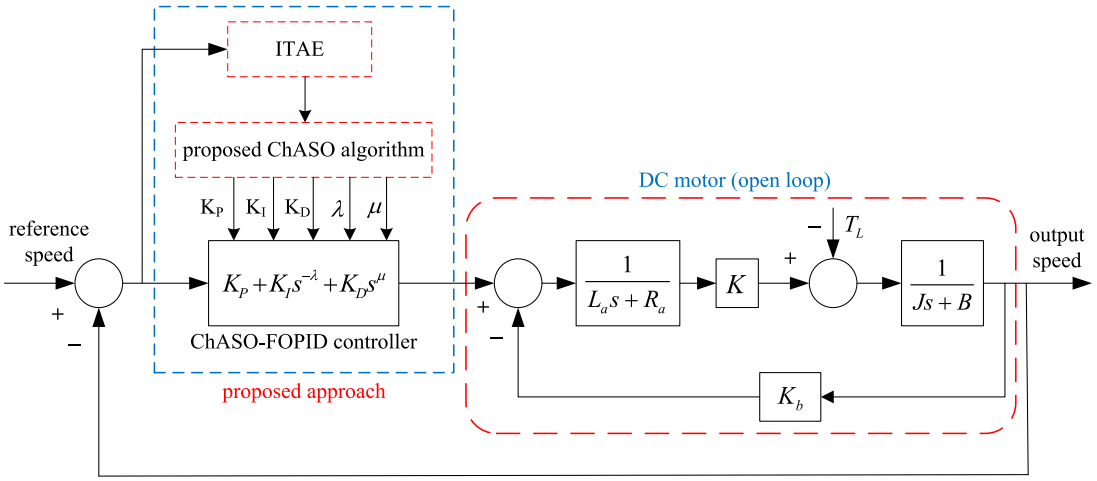

FIGURE 6. DC motor speed control with ChASO-FOPID controller.

The ITAE objective is given as

$$ITAE = \int_0^{t_{sim}} t \cdot |e(t)| \cdot dt \tag{34}$$

where $e(t)$ is the error signal that is the difference between reference and actual angular speeds, and t_{sim} is the simulation time, which is 2.0 s, in this paper. When the ITAE objective function is minimized, the transient response of the DC motor speed control system is improved in terms of maximum overshoot, settling time and rise time. The lower and upper limits of each FOPID controller parameters are $0.001 \leq K_P \leq 20, 0.001 \leq K_I \leq 20, 0.001 \leq K_D \leq 20$, $0 \leq \lambda \leq 2.0$ and $0 \leq \mu \leq 2.0$. These limits are identical to [38], [43], and [44] to be compared. In Oustaloup's approximation, $\omega_l = 10^{-3}\omega_c$, $\omega_h = 10^3\omega_c$, where ω_c is the transient gain frequency, and the order of approximation N is 11.

B. IMPLEMENTATION OF THE PROPOSED CHASO-FOPID APPROACH FOR DC MOTOR SPEED CONTROL

To improve the closed-loop response of the DC motor in terms of the transient response criteria (maximum overshoot, settling time and rise time), the optimal values of FOPID controller parameters can be found using the proposed ChASO algorithm, which has excellent exploitation and exploration capabilities compared to the original ASO algorithm. Fig. 6 illustrates the block diagram of the proposed ChASO-FOPID controller approach in DC motor speed control.

In order to optimize the five parameters of FOPID controller via the proposed ChASO algorithm, the parameters are first coded to an atom population such as $P = [K_P; K_I; K_D; \lambda; \mu]$, where each atom is represented by a real number. Then, the atoms are optimized by following the main steps of the ChASO algorithm to minimize the value of an objective function. In the proposed approach, the first population consists of randomly created m atoms (the population size). For each atom, the time domain simulation of the system with FOPID controller and unity feedback are made and the output speed curve of the DC motor is obtained. Each atom is likely to yield a different output speed response curve with the associated maximum overshoot, settling time and rise time values. After that, the ITAE objective function in (34) is calculated for each atom and the atoms are returned to the optimization module to be updated for the next iteration.

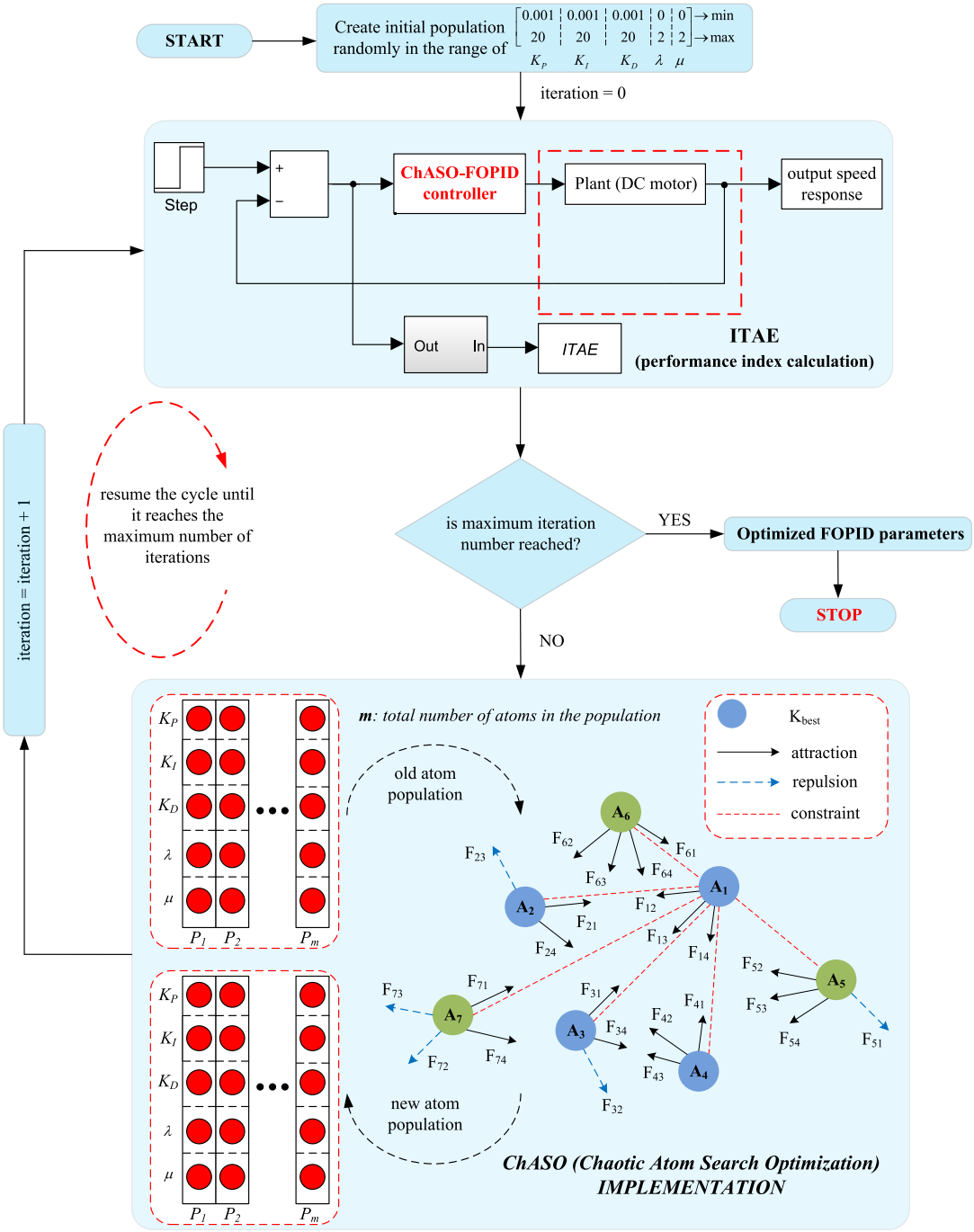

FIGURE 7. The block diagram of the proposed ChASO algorithm implementation for DC motor speed control.

This bidirectional process flow between the DC motor speed control system and the proposed ChASO optimization module is maintained until the maximum number of iterations is reached. At the end of the optimization process, the best atom with the lowest objective function value is recognized as the optimal FOPID parameter set. The detailed flow chart of the ChASO algorithm that is applied to optimize the performance of the DC motor speed control system is shown in Fig. 7.

VI. SIMULATION RESULTS AND DISCUSSIONS

The programming codes that is necessary for the ChASO algorithm and the simulations of the transient response, frequency response and robustness analyzes were all performed by means of the MATLAB/Simulink software package via a personal computer with Intel® i7 2.50 GHz processor and 16.00 GB RAM. The parameters of the proposed ChASO algorithm and their values are listed in Table 4.

TABLE 4. ChASO algorithm parameters.

Parameter	Value
Number of atoms (population)	50
δ, y (chaotic logistic map parameters)	4, 0.2027
α, β	50, 0.2
Maximum iteration number	30
Lower bounds for K_P, K_I, K_D, λ and μ	[0.001 0.001 0.001 0 0]
Upper bounds for K_P, K_I, K_D, λ and μ	[20 20 20 2 2]

In order to see the effectiveness and superiority of the proposed ChASO-FOPID approach, ChASO-FOPID controller is compared not only with the original ASO-based PID and FOPID (ASO-PID and ASO-FOPID) controllers accordingly but also with different approaches found in literature, using the same DC motor parameters (GWO-FOPID [38], GWO-PID [38], IWO-PID [43] and SFS-PID [44]). In addition, the best results in comparative analysis are highlighted in bold. The important results of this study are shown in the following subsections.

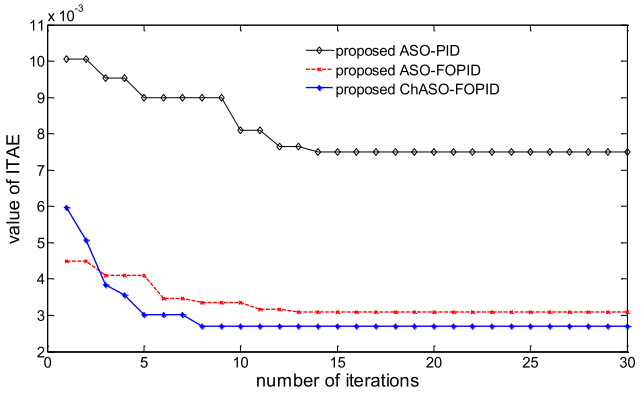

FIGURE 8. Convergence curves for ITAE objective function.

A. CONVERGENCE PROFILE

Fig. 8 shows the typical convergence profile of the proposed controller. As can be seen from the figure, the FOPID controller tuned by ChASO algorithm has the lowest ITAE value and converges with the least number of iterations (only 8 iterations). At the end of the optimization process the obtained ChASO-FOPID controller parameters are: $K_P = 19.7722$, $K_I = 9.1117$, $K_D = 8.1189$, $\lambda = 0.8401$, and $\mu = 0.9112$; and ASO-FOPID controller parameters are: $K_P = 19.3282$, $K_I = 7.9728$, $K_D = 4.7805$, $\lambda = 0.9755$, and $\mu = 0.9428$; and ASO-PID controller parameters are: $K_P = 11.9437$, $K_I = 2.0521$, and $K_D = 2.4358$. The transfer functions obtained according to these parameters are given in (35)-(37), as shown at the bottom of this page, respectively.

The speed step responses of the DC motor for ChASO-FOPID, ASO-FOPID and ASO-PID controllers are shown in Figs. 9-11, respectively. As can be seen from the figures, the proposed ChASO-FOPID controller has the best transient response profile as it performs a faster stability with no overshoot.

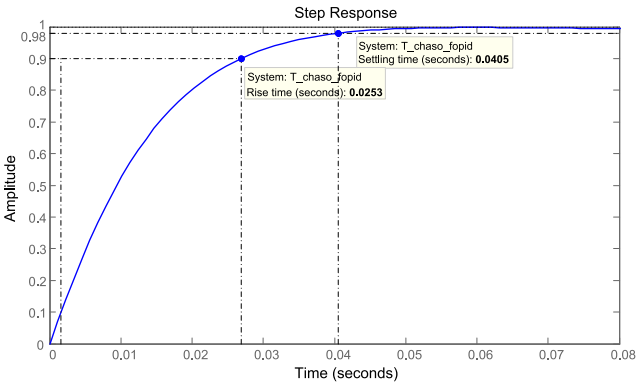

FIGURE 9. Speed step response of the DC motor with ChASO-FOPID controller.

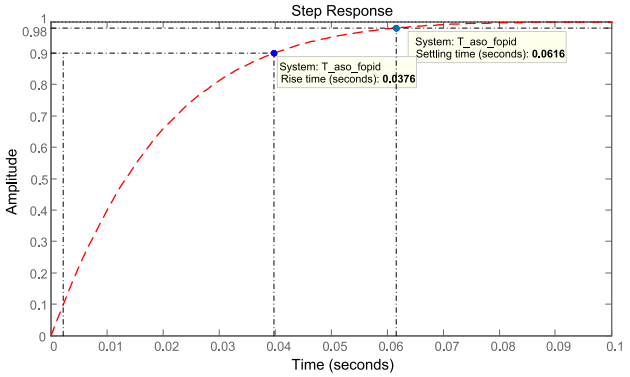

FIGURE 10. Speed step response of the DC motor with ASO-FOPID controller.

B. SPEED COMPARISON OF DC MOTOR WITH VARIOUS APPROACHES

The gain parameters of the PID and FOPID controllers obtained with different algorithms are listed in Table 5.

$$T_{ChASO-FOPID} = \frac{0.12178s^{1.7513} + 0.29658s^{0.8401} + 0.13668}{0.00108s^{2.8401} + 0.0061s^{1.8401} + 0.12178s^{1.7513} + 0.29821s^{0.8401} + 0.13668} \quad (35)$$

$$T_{ASO-FOPID} = \frac{0.071707s^{1.9183} + 0.28992s^{0.9755} + 0.11959}{0.00108s^{2.9755} + 0.0061s^{1.9755} + 0.071707s^{1.9183} + 0.29155s^{0.9755} + 0.11959} \quad (36)$$

$$T_{ASO-PID} = \frac{0.03654s^2 + 0.1792s + 0.03078}{0.00108s^3 + 0.04264s^2 + 0.1808s + 0.03078} \quad (37)$$

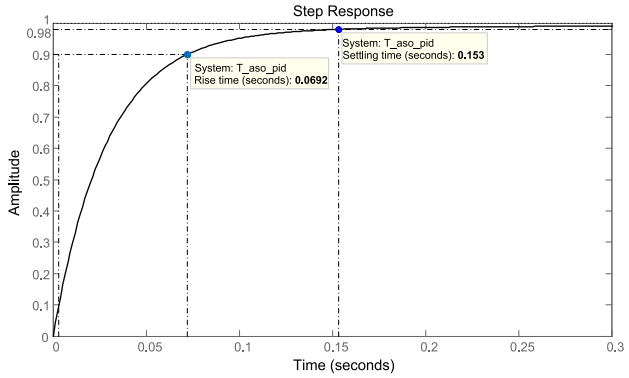

FIGURE 11. Speed step response of the DC motor with ASO-PID controller.

TABLE 5. Parameters of PID and FOPID controllers for DC motor obtained by various algorithms.

Algorithm-Controller	K_P	K_I	K_D	λ	μ
ChASO-FOPID (proposed)	19.7722	9.1117	8.1189	0.8401	0.9112
ASO-FOPID (proposed)	19.3282	7.9728	4.7805	0.9755	0.9428
ASO-PID (proposed)	11.9437	2.0521	2.4358	1	1
GWO-FOPID [38]	18.328	4.9418	3.2612	0.9998	0.9845
GWO-PID [38]	6.8984	0.5626	0.9293	1	1
IWO-PID [43]	1.5782	0.4372	0.0481	1	1
SFS-PID [44]	1.6315	0.2798	0.2395	1	1

TABLE 6. Comparison of the transient response analysis results for different controllers.

Algorithm-Controller	Overshoot (%)	Settling time (s) (±2%)	Rise time (s) (0.10→0.90)
ChASO-FOPID (proposed)	**No overshoot**	**0.0405**	**0.0253**
ASO-FOPID (proposed)	No overshoot	0.0616	0.0376
ASO-PID (proposed)	No overshoot	0.1535	0.0692
GWO-FOPID [38]	0.3145	0.0814	0.0488
GWO-PID [38]	1.5062	0.2052	0.1388
IWO-PID [43]	6.9759	1.2533	0.4189
SFS-PID [44]	No overshoot	1.4475	0.5436

In Table 6, comparative analysis of the proposed ChASO-FOPID approach with ASO-FOPID, ASO-PID, GWO-FOPID [38], GWO-PID [38], IWO-PID [43] and FS-PID [44] is shown in terms of the transient response measures. Also, the comparison of speed step responses for different controllers is shown in Fig. 12. As can be seen from the simulation results, the ChASO-FOPID controller designed for DC motor speed control has no overshoot with faster stability indices compared to PID and FOPID controllers that are optimized with different algorithms.

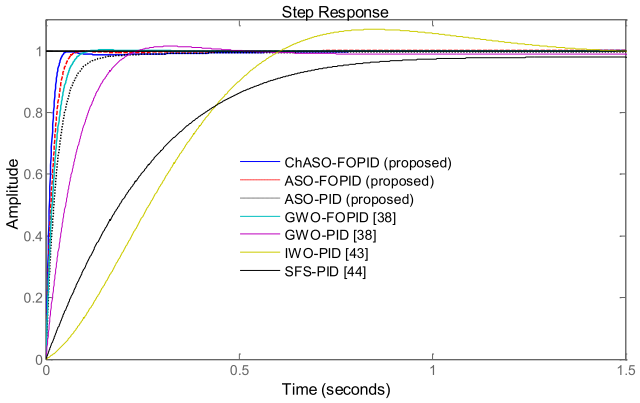

FIGURE 12. Speed step response comparison of DC motor with different controllers.

C. COMPARISON OF PERFORMANCE INDICES

ITSE and ZLG performance indices were also chosen for comparison because of their widespread use. The formulas of the ITSE and ZLG indices are given in (38) and (39), respectively [58]–[60].

$$ITSE = \int_0^{t_{sim}} t \cdot e^2(t) \cdot dt \tag{38}$$

$$ZLG = (1 - e^{-\beta}) \cdot (M_p + E_{ss}) + e^{-\beta} \cdot (t_s - t_r) \tag{39}$$

In (39) M_p, E_{ss}, t_s and t_r denotes the maximum overshoot, steady state error, settling time and rise time, respectively. The weight factor β is usually taken as 1.0 [58]. The transient response performance of a system is maximized when the ITSE and ZLG values are the lowest. The comparative values of ITSE and ZLG performance indices obtained from different approaches are given in Table 7. As can be seen from this table, ITSE and ZLG values of the proposed ChASO-FOPID controller are the lowest compared to the other approaches. These numerical results clearly demonstrate that the proposed ChASO algorithm is superior to other algorithms, including ASO, and that the FOPID controller is more efficient than the traditional PID controller.

TABLE 7. Performance indices comparison of different controllers.

Algorithm-Controller	ITSE value	ZLG value
ChASO-FOPID (proposed)	**5.4978E-05**	**0.0056**
ASO-FOPID (proposed)	9.0970E-05	0.0088
ASO-PID (proposed)	2.6210E-04	0.0310
GWO-FOPID [38]	1.3087E-04	0.0140
GWO-PID [38]	0.0014	0.0340
IWO-PID [43]	0.0267	0.3511
SFS-PID [44]	0.0179	0.3325

D. FREQUENCY RESPONSE ANALYSIS

In order to evaluate the stability performance of the DC motor speed control system that is designed by the proposed ChASO

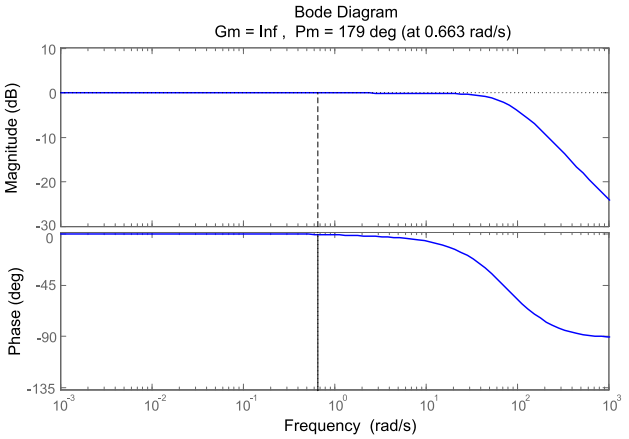

FIGURE 13. Bode plot of DC motor speed control system with ChASO-FOPID controller.

TABLE 8. Bode analysis of DC motor with different controllers.

Algorithm-Controller	Gain margin (dB)	Phase margin (deg.)	Bandwidth
ChASO-FOPID (proposed)	**Infinite**	**179.3515°**	**84.7989**
ASO-FOPID (proposed)	Infinite	178.3492°	57.0781
ASO-PID (proposed)	Infinite	180°	32.9113
GWO-FOPID [38]	Infinite	180°	44.0945
GWO-PID [38]	Infinite	180°	14.9018
IWO-PID [43]	Infinite	135.9149°	5.0987
SFS-PID [44]	Infinite	180°	4.1183

TABLE 9. Operating points of DC motor.

Case no.	R_a	K
(I)	0.20	0.009
(II)	0.20	0.021
(III)	0.60	0.009
(IV)	0.60	0.021

and ASO algorithms, the frequency response analysis were performed. The Bode plot for the proposed approach is shown in Fig. 13, and the comparative simulation results obtained for DC motor speed control system are given in Table 8. As seen from the table, ChASO-FOPID controller has the best performance with infinite gain margin, a phase margin close to 180° and the maximum bandwidth compared to other approaches. These results validate the effectiveness of the proposed ChASO algorithm for tuning of FOPID controller parameters.

E. ROBUSTNESS ANALYSIS

Robust controller is very much required for a system for maintaining the system's acceptable response in abnormal cases. The behavior of the system is observed by the robustness analysis when subjected to the system uncertainties. In this paper, in order to show the robustness of the proposed method, the electrical resistance (R_a) and the torque constant (K) of DC motor have been changed separately with ±50% and ±40%, respectively, which creates four possible operating points as given in Table 9. The comparative simulation results obtained for transient response analysis of DC motor speed control system for all operating points are given in Tables 10-13, and the comparative DC motor speed step response curves are given in Figs. 14-17. From these

TABLE 10. Comparison of transient response analysis results for Case I.

Algorithm-Controller	Overshoot (%)	Settling time (s) (±2%)	Rise time (s) (0.10→0.90)
ChASO-FOPID (proposed)	**No overshoot**	**0.0756**	**0.0419**
ASO-FOPID (proposed)	**No overshoot**	0.1063	0.0621
ASO-PID (proposed)	0.0133	0.2548	0.1176
GWO-FOPID [38]	0.5784	0.1310	0.0885
GWO-PID [38]	1.4423	0.3154	0.2157
IWO-PID [43]	5.9002	4.1872	0.6356
SFS-PID [44]	0.6306	1.3557	0.8340

TABLE 11. Comparison of transient response analysis results for Case II.

Algorithm-Controller	Overshoot (%)	Settling time (s) (±2%)	Rise time (s) (0.10→0.90)
ChASO-FOPID (proposed)	0.5256	**0.0282**	**0.0183**
ASO-FOPID (proposed)	0.3577	0.0650	0.0531
ASO-PID (proposed)	**No overshoot**	0.0982	0.0483
GWO-FOPID [38]	0.4392	0.0581	0.0350
GWO-PID [38]	2.0515	0.2672	0.1018
IWO-PID [43]	12.1203	1.0453	0.3148
SFS-PID [44]	**No overshoot**	0.6247	0.3781

TABLE 12. Comparison of transient response analysis results for Case III.

Algorithm-Controller	Overshoot (%)	Settling time (s) (±2%)	Rise time (s) (0.10→0.90)
ChASO-FOPID (proposed)	**No overshoot**	0.2168	**0.0422**
ASO-FOPID (proposed)	**No overshoot**	**0.1121**	0.0629
ASO-PID (proposed)	**No overshoot**	0.3177	0.1209
GWO-FOPID [38]	0.0529	0.1436	0.0902
GWO-PID [38]	**No overshoot**	0.3436	0.2236
IWO-PID [43]	0.6250	1.0551	0.6968
SFS-PID [44]	**No overshoot**	6.1575	1.0030

TABLE 13. Comparison of transient response analysis results for Case IV.

Algorithm-Controller	Overshoot (%)	Settling time (s) (±2%)	Rise time (s) (0.10→0.90)
ChASO-FOPID (proposed)	0.3985	**0.0285**	**0.0183**
ASO-FOPID (proposed)	0.1913	0.0438	0.0272
ASO-PID (proposed)	**No overshoot**	0.1058	0.0489
GWO-FOPID [38]	0.1645	0.0651	0.0531
GWO-PID [38]	1.3669	0.1558	0.1036
IWO-PID [43]	9.0808	1.6260	0.3250
SFS-PID [44]	**No overshoot**	4.2741	0.4071

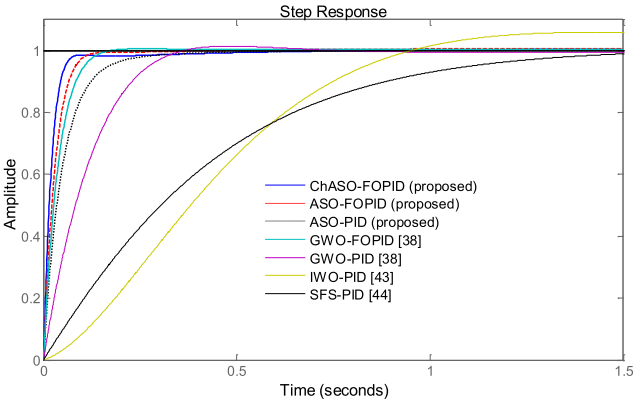

FIGURE 14. Comparative DC motor speed step response curves for Case I.

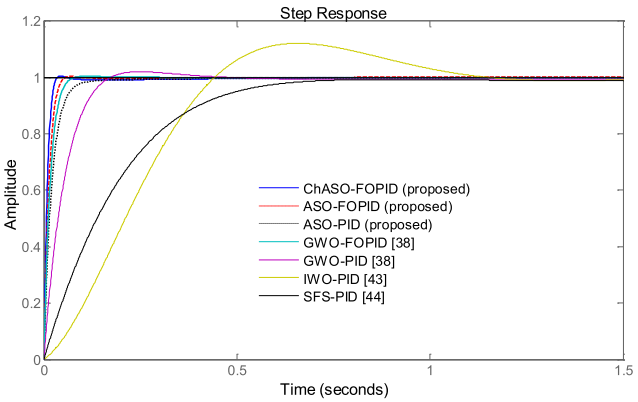

FIGURE 15. Comparative DC motor speed step response curves for Case II.

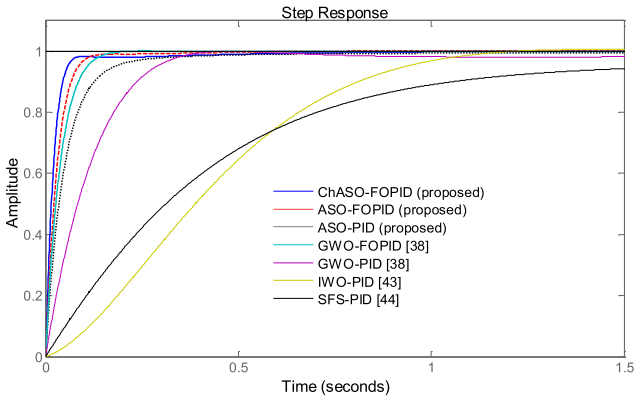

FIGURE 16. Comparative DC motor speed step response curves for Case III.

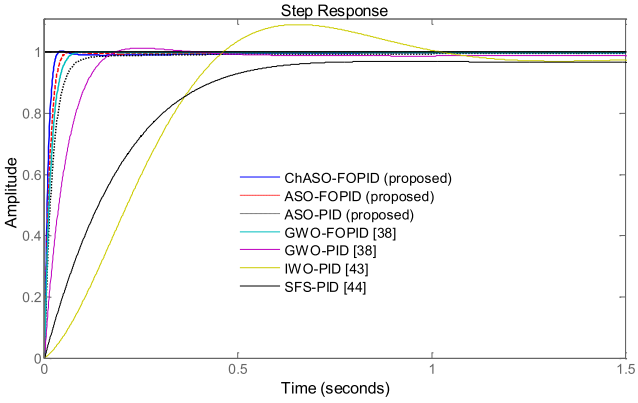

FIGURE 17. Comparative DC motor speed step response curves for Case IV.

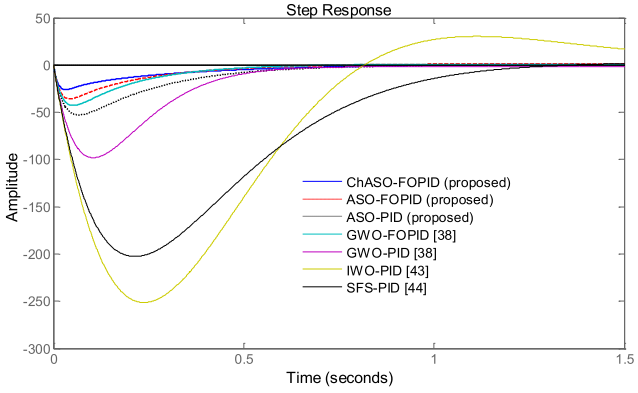

FIGURE 18. Step load disturbance response of DC motor.

tables and figures, it can be seen that despite the changes that occur in system parameters, the proposed ChASO-FOPID controller has the least settling time and rise time values with no overshoot in all cases except the Case II and Case IV with a negligible overshoot percentage when compared to all other controllers. These results validate the robustness of the proposed ChASO-FOPID controller for DC motor speed control system.

F. LOAD DISTURBANCE RESPONSE

This subsection presents the suppression capability of the closed loop DC motor speed control system with the proposed controllers as well as different controllers that are tested under the step load disturbance. When a change in load torque occurs in the DC motor speed control system, the output speed response of the system because of this disturbance, has to be settled down to zero as soon as possible. Fig. 18 shows

the dynamic response of the DC motor speed control for a step load disturbance. From the figure, it is clear that the proposed ChASO-FOPID controller has the best load disturbance response in terms of minimum undershoot and settling time, compared to the other controllers. Hence, the proposed controller is effective in successfully suppressing the load disturbances, as well.

VII. CONCLUSION

Tuning the parameters of FOPID controllers is a very challenging process. If the tuning success is insufficient, not only the control performances worsen, but also the control system becomes inefficient. In this study, the use of FOPID (ChASO-FOPID) controller based on the ChASO algorithm, which is developed by adding chaotic property to the original ASO algorithm, is proposed as a new approach in DC motor speed control. For DC motor speed control system with the FOPID controller and unity feedback, the ChASO algorithm was run to minimize the ITAE objective function and at the end of the optimization process the parameters of the FOPID controller were obtained with the least number of iterations. In order to demonstrate the effectiveness of the proposed ChASO-FOPID approach, performance comparisons were made not only with the original ASO tuned PID and FOPID (ASO-PID and ASO-FOPID) controllers, but also with recent approaches through various analyzes. As the recent approaches in the literature, GWO-FOPID [38], GWO-PID [38], IWO-PID [43] and SFS-PID [44] were selected since they have used the same DC motor model. The comparative analysis results showed that the proposed ChASO-FOPID controller added system had the best transient response profile and a good frequency response in terms of maximum overshoot, settling time, rise time, ITSE and ZLG. Furthermore, the ChASO-FOPID approach is more robust to model uncertainties than other approaches and more successful in suppressing the abrupt changes that may occur in the system output due to load disturbances.

REFERENCES

[1] B. Hekimoğlu, S. Ekinci, and S. Kaya, "Optimal PID controller design of DC-DC buck converter using whale optimization algorithm," in *Proc. IEEE IDAP*, Malatya, Turkey, Sep. 2018, pp. 1–6.

[2] S. Khubalkar, A. Junghare, M. Aware, and S. Das, "Modeling and control of a permanent-magnet brushless dc motor drive using a fractional order proportional-integral-derivative controller," *Turkish J. Elect. Eng. Comput. Sci.*, vol. 25, no. 5, pp. 4223–4241, 2017.

[3] I. Podlubny, "Fractional order systems and $PI^{\lambda}D^{\mu}$-controllers," *IEEE Trans. Autom. Control*, vol. 44, no. 1, pp. 208–214, Jan. 1999.

[4] S. Das, *Functional Fractional Calculus*, 2nd ed. New York, NY, USA: Springer, 2011.

[5] R. Caponetto, G. Dongola, L. Fortuna, and I. Petráš, *Fractional Order Systems: Modeling and Control Applications*. Singapore: World Scientific Publishing, 2010.

[6] C. A. Monje, Y. Chen, B. M. Vinagre, D. Xue, and V. Feliu-Batlle, *Fractional-order Systems and Controls: Fundamentals and Applications*. London, U.K.: Springer-Verlag, 2010.

[7] P. Shah and S. Agashe, "Review of fractional PID controller," *Mechatronics*, vol. 38, pp. 29–41, Sep. 2016.

[8] S. Khubalkar, A. Chopade, A. Junghare, M. Aware, and S. Das, "Design and realization of stand-alone digital fractional order PID controller for buck converter fed DC motor," *Circuits, Syst., Signal Process.*, vol. 35, no. 6, pp. 2189–2211, 2016.

[9] A. Khurram, H. Rehman, S. Mukhopadhyay, and D. Ali, "Comparative analysis of integer-order and fractional-order proportional integral speed controllers for induction motor drive systems," *J. Power. Electron.*, vol. 18, no. 3, pp. 723–735, 2018.

[10] H. S. Khaldi and A. C. Ammari, "Fractional-order control of three level boost DC/DC converter used in hybrid energy storage system for electric vehicles," in *Proc. 6th IREC*, Sousse, Tunisia, 2015, pp. 1–7.

[11] O. Atan, D. Chen, and M. Turk, "Fractional order PID and application of its circuit model," *J. Chin. Inst. Eng.*, vol. 39, no. 6, pp. 695–703, 2016.

[12] A. S. Chopade, S. W. Khubalkar, A. S. Junghare, M. V. Aware, and S. Das, "Design and implementation of digital fractional order PID controller using optimal pole-zero approximation method for magnetic levitation system," *IEEE/CAA J. Autom. Sinica*, vol. 5, no. 5, pp. 977–989, Sep. 2018.

[13] S. Das, S. Saha, S. Das, and A. Gupta, "On the selection of tuning methodology of FOPID controllers for the control of higher order processes," *ISA Trans.*, vol. 50, no. 3, pp. 376–388, 2011.

[14] X. Li, Y. Wang, N. Li, M. Han, Y. Tang, and F. Liu, "Optimal fractional order PID controller design for automatic voltage regulator system based on reference model using particle swarm optimization," *Int. J. Mach. Learn. Cybern.*, vol. 8, no. 5, pp. 1595–1605, 2017.

[15] D. Hu, Z. Qi, Y. Tang, and Y. He, "Research on fractional order PID controller applied to PEMFC pre-stage power conversion," in *Proc. 29th CCDC*, Chongqing, China, 2017, pp. 1015–1020.

[16] E. Sahin, M. S. Ayas, and I. H. Altas, "A PSO optimized fractional-order PID controller for a PV system with DC-DC boost converter," in *Proc. 16th PEMC*, Antalya, Turkey, 2014, pp. 477–481.

[17] R. Lahcene, S. Abdeldjalil, and K. Aissa, "Optimal tuning of fractional order PID controller for AVR system using simulated annealing optimization algorithm," in *Proc. 5th ICEE-B*, Boumerdes, Algeria, Oct. 2017, pp. 1–6.

[18] M. Çelebi and A. Başçi, "Fractional order control of a sinusoidal output inverter," *Istanbul Univ.-J. Elect. Electron. Eng.*, vol. 16, no. 2, pp. 3037–3042, 2016.

[19] M. T. Özdemir, D. Özturk, I. Eke, V. Çelik, and K. Y. Lee, "Tuning of optimal classical and fractional order PID parameters for automatic generation control based on the bacterial swarm optimization," *IFAC-PapersOnline*, vol. 48, no. 30, pp. 501–506, 2015.

[20] R. Caponetto, L. Fortuna, S. Fazzino, and M. G. Xibilia, "Chaotic sequences to improve the performance of evolutionary algorithms," *IEEE Trans. Evol. Comput.*, vol. 7, no. 3, pp. 289–304, Jun. 2003.

[21] L. dos Santos Coelho, "Tuning of PID controller for an automatic regulator voltage system using chaotic optimization approach," *Chaos, Solitons Fractals*, vol. 39, no. 4, pp. 1504–1514, 2009.

[22] N. S. Jaddi and S. Abdullah, "Optimization of neural network using kidney-inspired algorithm with control of filtration rate and chaotic map for real-world rainfall forecasting," *Eng. Appl. Artif. Intell.*, vol. 67, pp. 246–259, Jan. 2018.

[23] G. I. Sayed, G. Khoriba, and M. H. Haggag, "A novel chaotic salp swarm algorithm for global optimization and feature selection," *Appl. Intell.*, vol. 48, no. 10, pp. 3462–3481, 2018.

[24] S. Ahmed, M. Mafarja, H. Faris, and I. Aljarah, "Feature selection using salp swarm algorithm with chaos," in *Proc. ISMSI*, Phuket, Thailand, 2018, pp. 65–69.

[25] S. Arora and P. Anand, "Chaotic grasshopper optimization algorithm for global optimization," *Neural Comput. Appl.*, to be published. doi: 10.1007/s00521-018-3343-2.

[26] D. Oliva, M. Abd El Aziz, and A. E. Hassanien, "Parameter estimation of photovoltaic cells using an improved chaotic whale optimization algorithm," *Appl. Energy*, vol. 200, pp. 141–154, Aug. 2017.

[27] U. Guvenc, S. Duman, and Y. Hınıslıoglu, "Chaotic moth swarm algorithm," presented at the IEEE INISTA, Gdynia, Poland, 2017. doi: 10.1109/INISTA.2017.8001138.

[28] H. M. Zawbaa, E. Emary, and C. Grosan, "Feature selection via chaotic antlion optimization," *PLoS ONE*, vol. 11, no. 3, pp. 1–21, 2016. doi: 10.1371/journal.pone.0150652.

[29] S. Saremi, S. Mirjalili, and A. Lewis, "Biogeography-based optimisation with chaos," *Neural Comput. Appl.*, vol. 25, no. 5, pp. 1077–1097, 2014.

[30] A. H. Abdullah, R. Enayatifa, and M. Lee, "A hybrid genetic algorithm and chaotic function model for image encryption," *AEU–Int. J. Electron. Commun.*, vol. 66, no. 10, pp. 806–816, 2012.

[31] Q.-K. Pan, L. Wang, and L. Gao, "A chaotic harmony search algorithm for the flow shop scheduling problem with limited buffers," *Appl. Soft Comput.*, vol. 11, no. 8, pp. 5270–5280, 2011.
[32] E. Yalçın, M. C. Taplamacıoğlu, and E. Çam, "The adaptive chaotic symbiotic organisms search algorithm proposal for optimal reactive power dispatch problem in power systems," *Electrica*, vol. 19, no. 1, pp. 37–47, 2019.
[33] M. Kohli and S. Arora, "Chaotic grey wolf optimization algorithm for constrained optimization problems," *J. Comput. Des. Eng.*, vol. 5, no. 4, pp. 458–472, 2018.
[34] G. Kaur and S. Arora, "Chaotic whale optimization algorithm," *J. Comput. Des. Eng.*, vol. 5, no. 3, pp. 275–284, 2018.
[35] S. Mirjalili and A. H. Gandomi, "Chaotic gravitational constants for the gravitational search algorithm," *Appl. Soft Comput.*, vol. 53, pp. 407–419, Apr. 2017.
[36] G.-G. Wang, S. Deb, A. H. Gandomi, Z. Zhang, and A. H. Alavi, "Chaotic cuckoo search," *Soft Comput.*, vol. 20, no. 9, pp. 3349–3362, 2016.
[37] S. Saremi, S. Mirjalili, and S. Mirjalili, "Chaotic krill herd optimization algorithm," *Procedia Technol.*, vol. 12, pp. 180–185, Jan. 2014.
[38] J. Agarwal, G. Parmar, R. Gupta, and A. Sikander, "Analysis of grey wolf optimizer based fractional order PID controller in speed control of DC motor," *Microsyst. Technol.*, vol. 24, no. 12, pp. 4997–5006, 2018.
[39] R. V. Jain, M. V. Aware, and A. S. Junghare, "Tuning of fractional order PID controller using particle swarm optimization technique for DC motor speed control," in *Proc. 1st ICPEICES*, Delhi, India, 2016, pp. 1–4.
[40] A. Roy and S. Srivastava, "Design of optimal $PI^{\lambda}D^{\delta}$ controller for speed control of DC motor using constrained particle swarm optimization," in *Proc. IEEE ICCPCT*, Nagercoil, India, Mar. 2016, pp. 1–6.
[41] A. Madadi and M. M. Motlagh, "Optimal control of DC motor using grey wolf optimizer algorithm," *Tech. J. Eng. Appl. Sci.*, vol. 4, no. 4, pp. 373–379, 2014.
[42] U. Bhatnagar and A. Gupta, "Application of grey wolf optimization in optimal control of DC motor and robustness analysis," *Skit Res. J.*, vol. 8, no. 1, pp. 19–25, 2018.
[43] M. Khalilpuor, N. Razmjooy, H. Hosseini, and P. Moallem, "Optimal control of DC motor using invasive weed optimization (IWO) algorithm," in *Proc. Maclesi Conf. Elect. Eng.*, Isfahan, Iran, 2011, pp. 1–7.
[44] I. Khanam and G. Parmar, "Application of SFS algorithm in control of DC motor and comparative analysis," in *Proc. 4th UPCON*, Mathura, India, 2017, pp. 256–261.
[45] A. T. El-Deen, A. A. H. Mahmoud, and A. R. El-Sawi, "Optimal PID tuning for DC motor speed controller based on genetic algorithm," *Int. Rev. Autom. Control*, vol. 8, no. 1, pp. 80–85, 2015.
[46] B. Hekimoğlu, S. Ekinci, V. Demiray, R. Doguruci, and A. Yıldırım, "Speed control of DC motor using PID controller tuned by salp swarm algorithm," in *Proc. IENSC*, Diyarbakır, Turkey, 2018, pp. 1878–1889.
[47] R. K. Achanta and V. K. Pamula, "DC motor speed control using PID controller tuned by Jaya optimization algorithm," in *Proc. ICPCSI*, Chennai, India, 2017, pp. 983–987.
[48] A. K. Mishra, V. K. Tiwari, R. Kumar, and T. Verma, "Speed control of DC motor using artificial bee colony optimization technique," in *Proc. CARE*, Jabalpur, India, 2013, pp. 1–6.
[49] S. Ekinci, A. Demiroren, and B. Hekimoglu, "Parameter optimization of power system stabilizers via kidney-inspired algorithm," *Trans. Inst. Meas. Control*, vol. 41, no. 5, pp. 1405–1417, 2019.
[50] S. Ekinci, Optimal design of power system stabilizer using sine cosine algorithm, *J. Fac. Eng. Archit. Gaz*, to be published. doi: 10.17341/gazimmfd.460529.
[51] S. Ekinci and B. Hekimoğlu, "Multi-machine power system stabilizer design via HPA algorithm," *J. Fac. Eng. Archit. Gazi Univ.*, vol. 32, no. 4, pp. 1271–1285, 2017.
[52] W. Zhao, L. Wang, and Z. Zhang, "A novel atom search optimization for dispersion coefficient estimation in groundwater," *Future Gener. Comput. Syst.*, vol. 91, pp. 601–610, Feb. 2019.
[53] Z.-L. Gaing, "A particle swarm optimization approach for optimum design of PID controller in AVR system," *IEEE Trans. Energy Convers.*, vol. 19, no. 2, pp. 384–391, Jun. 2004.
[54] M. S. Tavazoei and M. Haeri, "An optimization algorithm based on chaotic behavior and fractal nature," *J. Comput. Appl. Math.*, vol. 206, pp. 1070–1081, Sep. 2007.
[55] K. Ogata, *System Dynamics*, 4th ed. Upper Saddle River, NJ, USA: Prentice-Hall, 2004.
[56] Y. Tang, M. Cui, C. Hua, L. Li, and Y. Yang, "Optimum design of fractional order $PI^{\lambda}D^{\mu}$ controller for AVR system using chaotic ant swarm," *Expert Syst. Appl.*, vol. 39, no. 8, pp. 6887–6896, 2012.
[57] A. Oustaloup, F. Levron, B. Mathieu, and F. M. Nanot, "Frequency-band complex noninteger differentiator: Characterization and synthesis," *IEEE Trans. Circuits Syst. I, Fundam. Theory Appl.*, vol. 47, no. 1, pp. 25–39, Jan. 2000.
[58] B. Hekimoğlu, "Sine-cosine algorithm-based optimization for automatic voltage regulator system," *Trans. Inst. Meas. Control*, vol. 41, no. 6, pp. 1761–1771, 2019. doi: 10.1177/0142331218811453.
[59] B. Hekimoğlu and S. Ekinci, "Grasshopper optimization algorithm for automatic voltage regulator system," in *Proc. 5th ICEEE*, Istanbul, Turkey, 2018, pp. 152–156.
[60] S. Ekinci, B. Hekimoğlu, and S. Kaya, "Tuning of PID controller for AVR system using salp swarm algorithm," in *Proc. IDAP*, Malatya, Turkey, 2018, pp. 1–6.

Authors' photographs and biographies not available at the time of publication.